Note: All citation numbers refer to the list of references at the end of this Supplement, not to the list of references in the main text.

Testing consistency of the model

In the model, ions are charged, hard spheres and water is a fluid of hard spheres, all moving through RyR via one-dimensional drift-diffusion (PNP). Selectivity occurs when the ions interact with the five amino acids described in the main text (Asp-4899, Glu-4900, Asp-4938, Asp-4945, and Glu-4902). Figs. S1–S9 in this Supplement show how the results of this model compare to experiments. Given how well the model reproduces the experimental data and that it can predict other data, this minimalist model seems to capture the essential physics of ion permeation and selectivity in RyR. On the other hand, the model does not include several energies usually included in other models of ion permeation and selectivity. At the same time, the diffusion coefficients seem unusually small. It is important to check the consistency of the model with respect to these issues:

Water as hard spheres. This model of water can reproduce relatively accurate values of the bath activity coefficients (Appendix of Ref. 1) which is important to reproduce the reversal potentials of the current/voltage curves. It does not, however, have any attractive ion/water interactions. The success of the model in reproducing the experimental data then suggests that there is only a small net energy step from ion dehydration as the ion enters the channel and resolvation by the COO^- of the protein charges. This is consistent with the experimental data of Mg^{2+} and Ca^{2+} and their mixtures with K^+. Fig. S9A and D shows that as more and more divalent is added to the lumenal side, the conductances at negative voltages are very similar; they differ by at most 10% at 50 mM divalent. If dehydration/resolvation were very important, it would show in this experiment since Mg^{2+} and Ca^{2+} have a 130 kT difference in dehydration energy (2). For example, at 5 mM divalent (Fig. S9A and D, solid squares), the current/voltage curves of Mg^{2+} and Ca^{2+} mixtures with K^+ are virtually identical, indicating the Mg^{2+} does not have difficulty entering the channel compared to Ca^{2+}; they both compete equally well with K^+. Gouaux and MacKinnon have suggested that a highly-charged selectivity filter can resolvate the ions to overcome any dehydration penalty (3); the net energy of an ion entering the pore is the sum of two terms that virtually cancel. The prediction of the model that the ion dehydration/resolvation step is small must be tested and will be explored in future work. If true, it is likely that this true only for RyR and a small number of other channels.

The dielectric coefficient of the entire system is 78.4. It is reasonable to assume that the dielectric coefficient of both the channel lumen and the channel protein is less (and possibly significantly less) than 78.4. Via Born energies, a low dielectric in the lumen is equivalent to an ion dehydration/resolvation penalty which, empirically, seems to be small; the dielectric coefficient within the pore seems to be high in this 8 Å-wide channel. An alternate explanation is that the screening component of the chemical potential includes a Born-like energy. In the mean spherical approximation of ions in bulk solutions (Eq. (16) of Ref. 4), the screening term is (to first-order) proportional to z_i^2 and inversely proportional to an effective ion radius—just like the Born energy. How much this compensation may be is difficult to estimate before more detailed studies on ion dehydration/resolvation are done.

On the other hand, a high protein dielectric coefficient is consistent with RyR having millimolar Ca^{2+} affinity (5,6) since a low-dielectric protein significantly increases Ca^{2+} affinity. This counter-intuitive result is due to the charges that ions induce on the protein/lumen dielectric interface. Boda et al. (5,6) have shown that in a highly-charged selectivity filter like in RyR, the

negative protein charges induce negative charges on this interface that attract more cations. In these simulations, the number of ions inside the pore changed by a factor 2–3 at millimolar [Ca^{2+}] when the protein dielectric constant had a value between 2 and 10. However, these low protein dielectric constants increased Ca^{2+} affinity by 5- to 10-fold beyond RyR's millimolar affinity (5,6). Therefore, it is likely that the RyR protein dielectric constant is not significantly smaller than the 78.4 used in the RyR model (probably 40 or above). The Boltzmann factor of an error due to the protein dielectric constant will thus be small (<1 kT for a 50% error in pore concentrations). As with any net change in Boltzmann factor, some terms in the chemical potential (e.g., excluded-volume) will become more positive and other terms (e.g., screening) will become more negative. Work is currently underway to incorporate different dielectric coefficients into the DFT.

The diffusion coefficients are very small. In the Appendix of the main text, a back-of-the-envelope calculation is presented that shows that a one-dimensional PNP approach where diffusion is limited in a highly-charged selectivity filter necessarily requires the very small diffusion coefficients used in the model. The calculation does not, however, indicate whether those diffusion coefficients are physically real. The diffusion coefficients of ions inside a highly-charged channel are currently not known. Only diffusion coefficients in weakly-charged pores have been computed by molecular dynamics (7-9). Work is currently under way to compute diffusion coefficients in a narrow DDDD locus.

The calculation in the Appendix also does not indicate whether the assumptions of the model are true; for example, in the model of Corry et al. (10) flux is not only limited in the selectivity filter, but also in one of the vestibules with a dielectric barrier. It may also be that approximations in the model are compensated for by the diffusion coefficients. For example, in the Nernst-Planck equation (Eq. (1) of the main text), it is the product $D_i\rho_i$ that appears, and therefore an incorrect density may be compensated for by an effective diffusion coefficient. This is certainly a possibility. However, charge neutrality gives a good upper bound on ρ_i. The protein charge density is large in RyR (13 M for Asp-4899) and diffusion is limited in a only 15 Å-long segment of the pore. In that case, the measured 800 pS conductance for K^+ can only be achieved in a one-dimensional PNP theory with a diffusion coefficient around 4% of bulk (see Appendix of main text). By this estimate, any error compensation there is seems to be limited to a factor significantly less than 10, or a Boltzmann factor of less than 2 kT. Certainly, they are the *effective* diffusion coefficients needed in such a model.

References (Supplementary Material)

1. Gillespie, D., L. Xu, Y. Wang, and G. Meissner. 2005. (De)constructing the ryanodine receptor: Modeling ion permeation and selectivity of the calcium release channel. J. Phys. Chem. B 109:15598-15610.

2. Fawcett, W. R. 1999. Thermodynamic Parameters for the Solvation of Monatomic Ions in Water. J. Phys. Chem. B 103:11181-11185.

3. Gouaux, E. and R. MacKinnon. 2005. Principles of Selective Ion Transport in Channels and Pumps. Science 310:1461-1465.

4. Nonner, W., L. Catacuzzeno, and B. Eisenberg. 2000. Binding and Selectivity in L-Type Calcium Channels: A Mean Spherical Approximation. Biophys. J. 79:1976-1992.

5. Boda, D., M. Valiskó, B. Eisenberg, W. Nonner, D. J. Henderson, and D. Gillespie. 2006. The effect of protein dielectric coefficient on the ionic selectivity of a calcium channel. J. Chem. Phys. 125:034901.

6. Boda, D., M. Valiskó, B. Eisenberg, W. Nonner, D. J. Henderson, and D. Gillespie. 2007. Combined effect of pore radius and protein dielectric coefficient on the selectivity of a calcium channel. Phys. Rev. Lett. 98:168102.

7. Smith, G. R. and M. S. P. Sansom. 1998. Dynamic Properties of Na^+ Ions in Models of Ion Channels: A Molecular Dynamics Study. Biophys. J. 75:2767-2782.

8. Mamonov, A. B., M. G. Kurnikova, and R. D. Coalson. 2006. Diffusion constant of K+ inside Gramicidin A: A comparative study of four computational methods. Biophys. Chem. 124:268-278.

9. Allen, T. W., S. Kuyucak, and S.-H. Chung. 2000. Molecular dynamics estimates of ion diffusion in model hydrophobic and KcsA potassium channels. Biophys. Chem. 86:1-14.

10. Corry, B., T. W. Allen, S. Kuyucak, and S.-H. Chung. 2001. Mechanisms of Permeation and Selectivity in Calcium Channels. Biophys. J. 80:195-214.

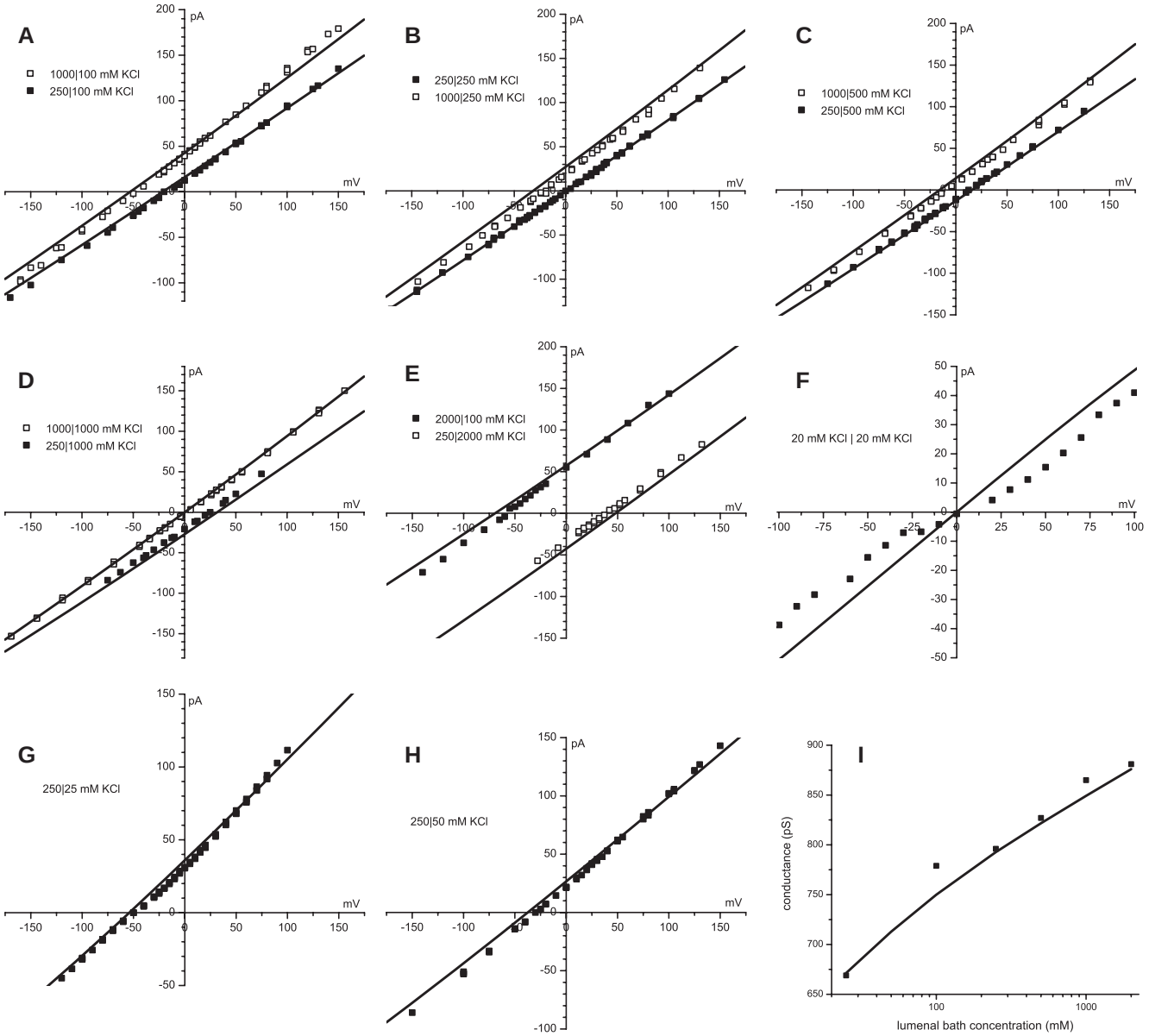

Figure S1. (A-H) Current/voltage curves in KCl. (I) The conductance at reversal potential with cytosolic [K^+] held at 250 mM and lumenal [K^+] is varied. For both experiment and theory the current/voltage curve was fitted with a line and the slope is plotted.

In this and the following figures, concentrations are listed as cytosolic | lumenal. The solid lines are the model and symbols are the experimental data. Comparing panel I and Fig. 16B of the original model (*J. Phys. Chem. B* 109:15598-15610) summarizes the improvements due to the new RyR model; in general the computed current/voltage curves are more linear and the conductances are significantly closer to experimental values, especially in cases where the lumenal concentration is low. With the exception of panel F, this experimental data was previously published by Chen et al. (*Biophys. J.* 73:1337-1354). The data in panel F was previously published by Gillespie et al. (*J. Phys. Chem. B* 109:15598-15610).

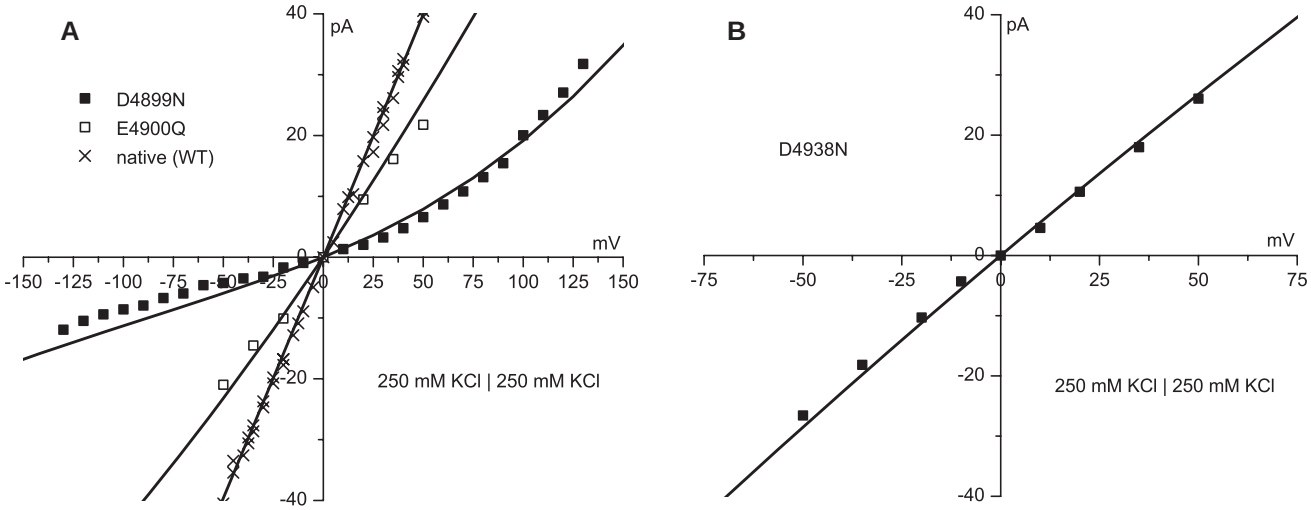

Figure S2. Current/voltage curves of (A) native (WT) RyR (×) and the mutants D4899N (■) and E4900Q (□) and (B) the D4938N mutant in 250 mM symmetric KCl. The D4899N data was previously published by Gao et al. (*Biophys. J.* 79:828-840), E4900Q by Wang et al. (*Biophys. J.* 89:256-265), and D4938N by Xu et al. (*Biophys. J.* 90:443-453).

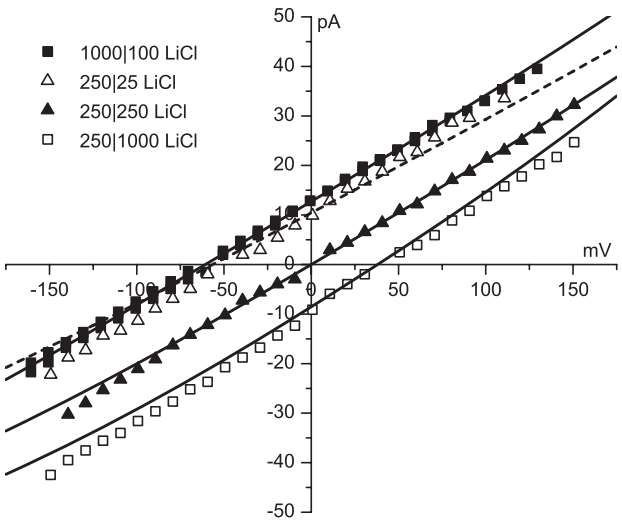

Figure S3. Current/voltage curves in LiCl. The dashed line is the model result for 250 mM cytosolic and 25 mM lumenal bath concentrations (Δ). Compared to the previous model, the dashed line reproduces the data much better. This experimental data was previously published by Chen et al. (*Biophys. J.* 76:1346-1366).

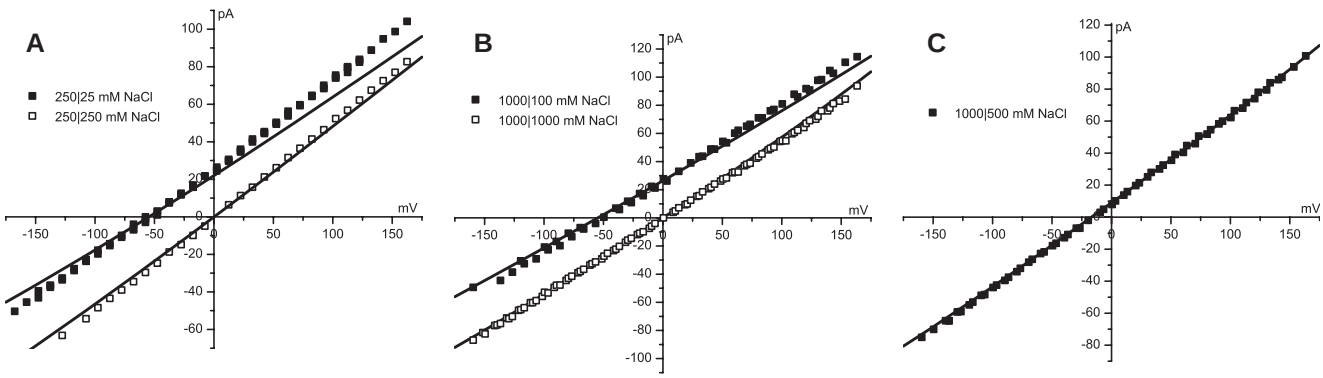

Figure S4. Current/voltage curves in NaCl. Compared to the previous model, the current/voltage curves are more linear and reproduce the data better in very asymmetric solutions. This experimental data was previously published by Chen et al. (*Biophys. J.* 76:1346-1366).

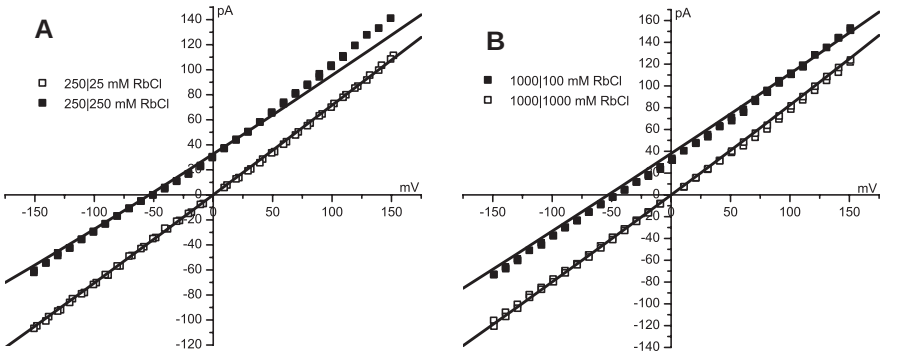

Figure S5. Current/voltage curves in RbCl. Compared to the previous model, the current/voltage curves are more linear and reproduce the data better in very asymmetric solutions. This experimental data was previously published by Chen et al. (*Biophys. J.* 76:1346-1366).

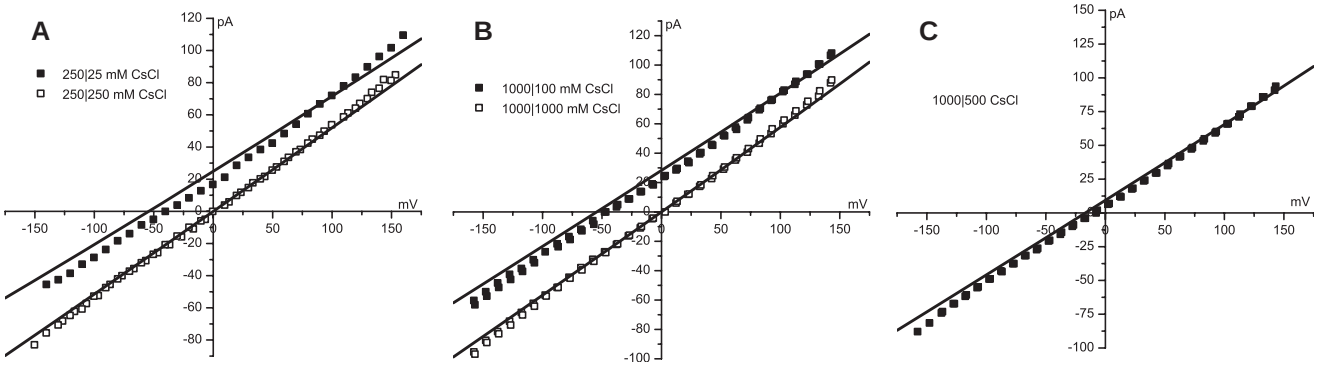

Figure S6. Current/voltage curves in CsCl. Compared to the previous model, the current/voltage curves are more linear and reproduce the data better in very asymmetric solutions. This experimental data was previously published by Chen et al. (*Biophys. J.* 76:1346-1366).

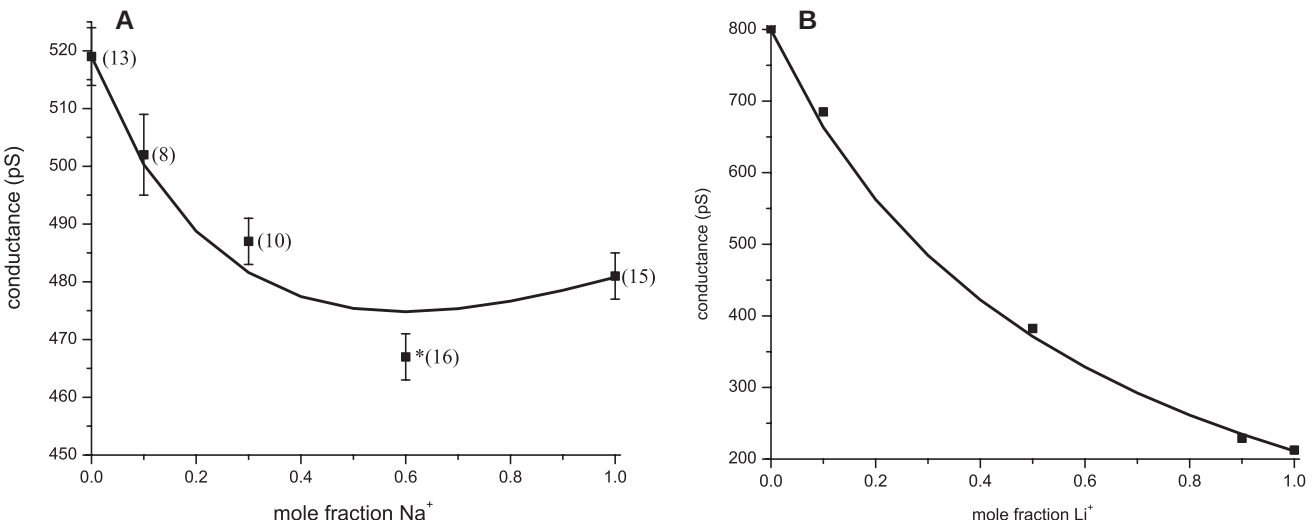

Figure S7. Mole fraction experiments at 250 mM total cation concentration in symmetric solutions. (A) NaCl and CsCl mixtures. The experimental point at mole fraction 0.6 is statistically significantly different than the point at mole fraction 1 ($p < 0.05$). The number of experiments is shown in parentheses. This experimental data was previously published by Gillespie et al. (*J. Phys. Chem. B* 109:15598-15610), but this is the first publication of this data with multiple experiments. (B) LiCl and KCl mixtures. This experimental data at these concentrations was previously published by Chen et al. (*Biophys. J.* 76:1346-1366). This mole fraction experiment was first performed at 210 mM total cation concentration by Lindsay et al. (*J. Physiol. (London)* 439:463-480).

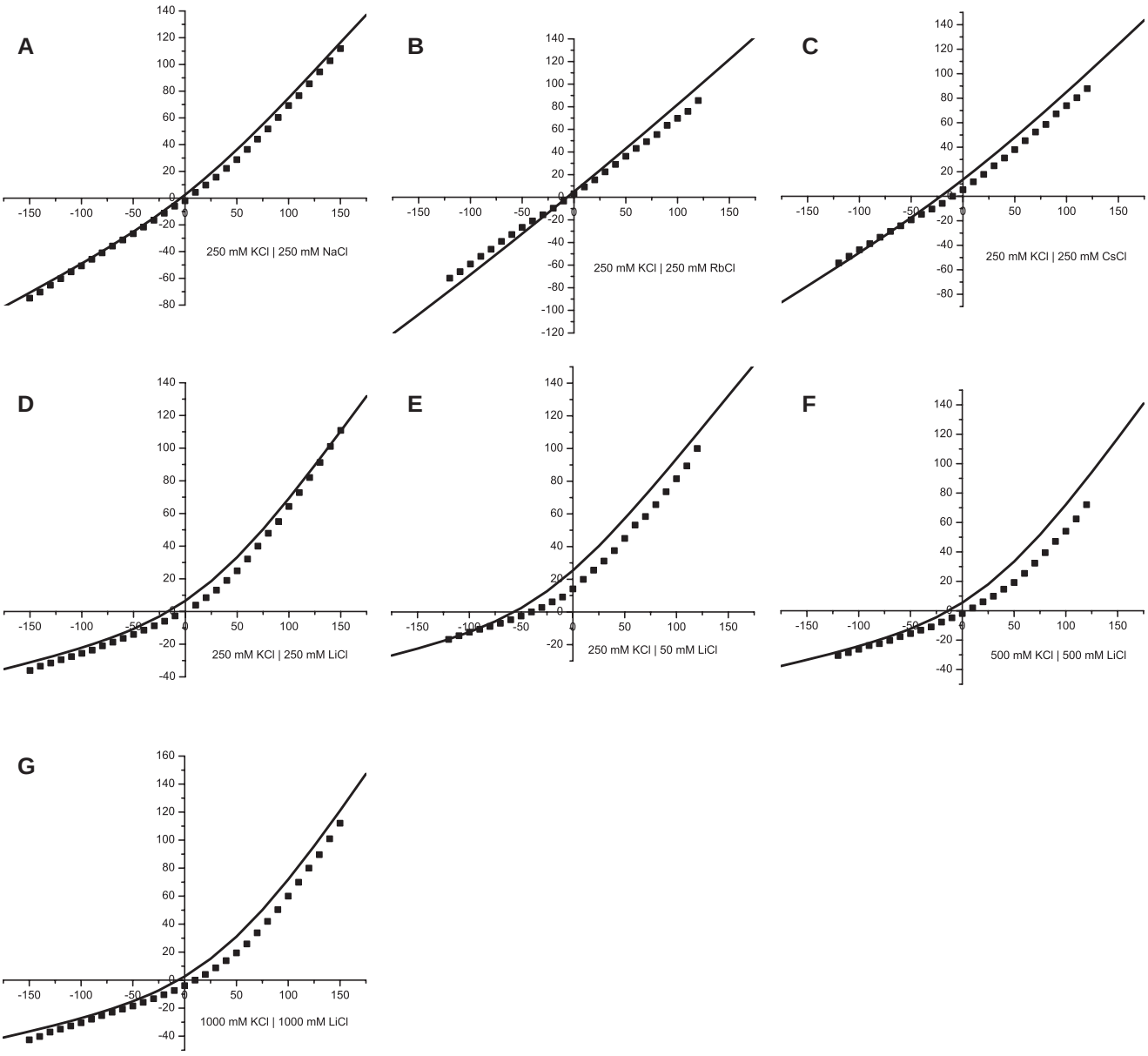

Figure S8. Current/voltage curves in bi-ionic conditions. This experimental data was previously published by Chen et al. (*Biophys. J.* 76:1346-1366).

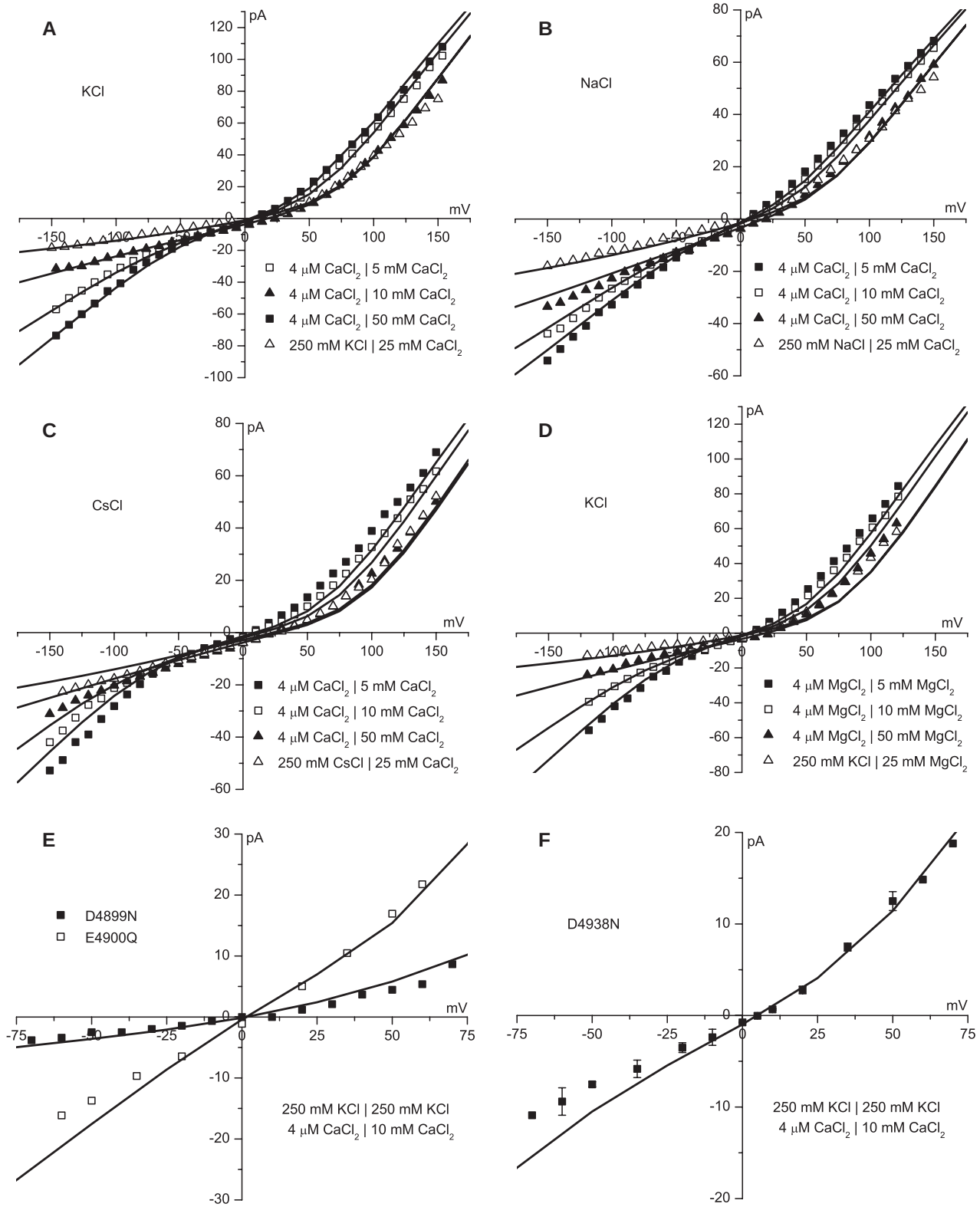

Figure S9. Current/voltage curves with divalent and monovalent cations. (A) KCl and $CaCl_2$. (B) NaCl and $CaCl_2$. (C) CsCl and $CaCl_2$. (D) KCl and $MgCl_2$. In both baths are 250 mM monovant-Cl and in the lumenal bath is 5 mM (■), 10 mM (□), and 50 mM (▲) divalent-Cl_2; or the cytosolic bath contains 250 mM cytosolic monovant-Cl while the lumenal bath contains 25 mM lumenal divalent-Cl_2 (Δ). Current/voltage curves of (E) the D4899N (■) and E4900Q (□) mutants and (F) the D4938N mutant in 250 mM symmetric KCl and 10 mM lumenal $CaCl_2$. Compared to the previous model, the current/voltage curves of Cs^+/Ca^{2+} mixtures and Na^+/Ca^{2+} mixture reproduce the data better. The data in panels A–D were first published by Chen et al. (*J. Phys. Chem. B* 107:9139-9145). The D4899N data (panel E) was previously published by Gao et al. (*Biophys. J.* 79:828-840), E4900Q (panel E) by Wang et al. (*Biophys. J.* 89:256-265), and D4938N (panel F) by Xu et al. (*Biophys. J.* 90:443-453).